Catalysis Letters (2024) 154:5171–5183
https://doi.org/10.1007/s10562-024-04686-y

# Promotion of $Mg(OH)_2$ in Cu-Based Catalysts for Selective Hydrogenation of Acetylene

Jiaming Liu[1,2] · Aonan Zeng[1,2] · Bo Xu[1,2] · Yao Wang[1,2] · Zhichao Sun[1,2] · Yingya Liu[1,2] · Wei Wang[3] · Anjie Wang[1,2]

Received: 22 February 2024 / Accepted: 15 April 2024 / Published online: 6 June 2024


## Abstract

The selective hydrogenation of acetylene is of industrially indispensable in the production of polymer-grade ethylene. The design of non-precious metal catalysts with outstanding performance is of pivotal importance in order to replace the supported Pd–Ag catalysts. Our previous work showed that a copper carbide ($Cu_xC$)-containing catalyst exhibited high hydrogenation activity and selectivity under mild conditions. In the present work, $Mg(OH)_2$ was used to modify the $Cu_xC$-containing catalyst in order to improve its catalytic performance. $Mg(OH)_2$-modified $Cu_xC$-containing catalyst was prepared from a coprecipitate of $Cu(OH)_2$ and $Mg(OH)_2$, which was obtained by precipitation of $Cu(NO_3)_2$ and $Mg(NO_3)_2$ solution with dropwise addition of NaOH solution, by thermal treatment in $C_2H_2$/Ar (0.5%) at 120 ℃ followed by $H_2$ reduction at 150 ℃. The introduction of $Mg(OH)_2$ led to reduced $Cu_xC$ crystalline size and to increased amount of $Cu_xC$ crystallites. In addition, the basic nature of $Mg(OH)_2$ is favorable to suppress the undesired oligomerization. The prepared catalyst showed excellent catalytic performance with complete acetylene conversion, low selectivity to unwanted ethane (24%), and high stability at 100 °C and atmospheric pressure in the presence of large excess ethylene in 100 h.

### Graphical Abstract

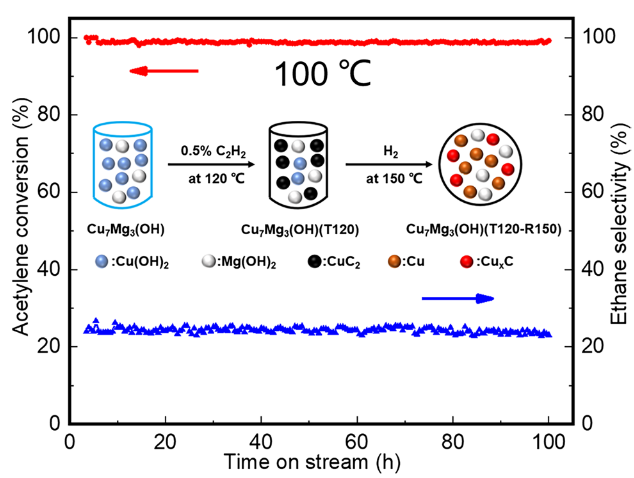


**Keywords** Magnesium hydroxide · Copper hydroxide · Copper carbide · Selective hydrogenation · Acetylene

✉ Yao Wang
wangyao@dlut.edu.cn

✉ Anjie Wang
ajwang@dlut.edu.cn

[1] State Key Laboratory of Fine Chemicals, School of Chemical Engineering, Dalian University of Technology, Dalian, Liaoning 116024, P. R. China

[2] Liaoning Key Laboratory of Petrochemical Technology and Equipments, Dalian University of Technology, Dalian, Liaoning 116024, P. R. China

[3] School of Chemical and Biological Engineering, Yinchuan University of Energy, Yinchuan, Ningxia 750105, P. R. China

## 1 Introduction

Ethylene is industrially used in the production of polymers, and the ethylene produced by cracking of naphtha contains about 1% acetylene impurity. A trace amount of acetylene in the ethylene feedback results in poisoning the Ziegler–Natta catalyst in the downstream ethylene polymerization, degrading the polymer product. As a consequence, the acetylene content in ethylene must be reduced to less than 5 ppm. Selective hydrogenation of acetylene to ethylene is regarded as an efficient, economical, and environmentally friendly method to remove acetylene impurity in industry [1–5]. Supported Pd–Ag catalysts are widely used for selective hydrogenation of acetylene due to their high activity and reasonable selectivity [6–10]. However, at near complete conversion of acetylene, an ethylene loss frequently occurs without co-feeding CO, which adsorbs stronger than ethylene but weaker than acetylene, because of the over-hydrogenation of ethylene to yield ethane. Moreover, supported Pd–Ag catalyst often produces green oil, which is generated by oligomerization, leading to gradual deactivation of the catalysts [8, 11–15]. Therefore, it is highly desirable to develop high-performance catalysts with reduced selectivity to undesired ethane and green oil.

To improve the performance of Pd-based catalysts, promoters such as Ag [16–19], Cu [20–22], Mg [23–26], Zn [27, 28], Ga [29, 30], Co [31, 32], and In [33, 34] are often added. Most of them tune the catalytic performance by forming intermetallic alloys with Pd, which have ordered crystal structures and provide unique and uniform active sites [16–20, 22, 27, 28, 30–33]. As for Mg species, they usually act as supports in the form of MgO [23–25]. Yuan et al. [23] prepared a 3D-Al-Pd/MMO catalyst derived from an Al-LDH containing Mg species, which demonstrated high activity, excellent selectivity as well as long-term stability for selective hydrogenation of acetylene to ethylene. Qin et al. [24] prepared a Pd/MgO catalyst with low loading of Pd (7.8 ppm) for selective hydrogenation of acetylene to ethylene, and the catalyst showed outstanding performance. Guo et al. [25] developed a single-atom Pd catalyst supported by MgO using a ball-milling method, and the prepared catalyst showed good catalytic performance for selective hydrogenation of acetylene to ethylene in excess ethylene. He et al. [30] prepared Pd–Ga/MgO-$Al_2O_3$ catalysts with high activity and high selectivity in selective hydrogenation of acetylene, owing to high dispersion and synergistic effect of bimetallic nanoalloys. Lomonosov et al. [26] synthesized bimetallic Pd-Mg nanoparticles by partial galvanic replacement of plasmonic Mg nano-particles, which exhibited a much higher ethylene selectivity than Pd alone in selective hydrogenation of acetylene. The improved catalytic behavior was attributed to the well-separated Pd nanoparticles on Mg, due to the ability of suppressing Pd aggregation. However, since Pd is scarce and expensive, there is ample room for improving the cost-effectiveness in catalyst design by finding a non-precious metal, such as Ni [35, 36] and Cu [37–39], to replace Pd-based catalysts [40].

In our previous work, it was found that a novel phase, copper carbide ($Cu_xC$), derived from copper acetylide showed high hydrogenation activity at low temperatures, comparable to Pd-based catalysts [41–47]. The $Cu_xC$-containing catalysts were prepared from a variety of copper precursors, including $Cu_2O$ [41], $Cu(OH)_2CO_3$ [42], $Cu(OH)_2$ [43] and CuO [44], by thermal treatment with acetylene-containing gas followed by hydrogen reduction. Cu-based catalysts are highly selective in hydrogenation of acetylene because the adsorption of acetylene is significantly stronger than that of ethylene [38, 48]. The precious-metal-like hydrogenation activity is attributed to the interstitial $Cu_xC$, whereas the porous carbonaceous shell layer, generated from the thermal decomposition of intermediate copper acetylide, blocked the chain growth of linear oligomers, thus suppressing the formation of green oil [41–44].

In the present work, $Mg(OH)_2$ species was used to modify the $Cu_xC$-containing catalyst. The prepared $Mg(OH)_2$-modified catalysts were tested in selective hydrogenation of acetylene with enhanced performance. The characterization results confirmed that the introduction of $Mg(OH)_2$ resulted in increased amount and reduced size of $Cu_xC$ crystallites. In addition, the presence of basic $Mg(OH)_2$ decreased the production of $C_4^=$, among which 1,3-butadiene is regarded as the precursor of green oil.

## 2 Experimental

### 2.1 Chemical Reagents

$Cu(NO_3)_2 \cdot 3H_2O$ was purchased from Guangdong Guanghua Sci-Tech CO., Ltd, China. $Mg(NO_3)_2 \cdot 6H_2O$ was purchased from Tianjin Damao Chemical Reagent Factory, China. NaOH was purchased from Tianjin Kemiou Chemical Reagent CO., Ltd, China. All reagents were of analytical grade and used without further purification. Hydrogen gas was purchased from Dalian Kena Science and Technology Co., Ltd, China. The reaction gas (0.8% $CH_4$, 0.5% $C_2H_2$, and 98.7% $C_2H_4$) and the treatment gas (0.5% $C_2H_2$, 99.5% Ar) were purchased from Dalian Guangming Chemical Research Institute, China.

### 2.2 Synthesis of Catalyst Precursors

The catalyst precursors were prepared by coprecipitation. $Cu(NO_3)_2 \cdot 3H_2O$ and $Mg(NO_3)_2 \cdot 6H_2O$ (the total amount of $Cu^{2+}$ and $Mg^{2+}$ was 0.02 mol, and $Mg^{2+}/Cu^{2+} = n/(10-n)$, n = 0–4) were dissolved in 200 mL deionized water and stirred for 30 min in an ice-water bath. Then 20 mL NaOH solution (2 mol/L) was added dropwise to the above solution. The resultant suspension was stirred for 30 min. The resultant blue suspension was filtered, and the solid was washed with deionized water and dried in vacuum at room temperature for 12 h to obtain the catalyst precursor, which is denoted as $Cu_{10-n}Mg_n(OH)$ (n = 0–4).

### 2.3 Catalyst Preparation

0.1 g $Cu_{10-n}Mg_n(OH)$ precursor was treated in a flow of acetylene-containing gas (0.5% $C_2H_2$/99.5% Ar, 30 mL/min) at 100–180 °C for 2 h, and then cooled down to room temperature. The obtained material was denoted as $Cu_{10-n}Mg_n(OH)$(Tx), where x represents the treatment temperature. Subsequently, $Cu_{10-n}Mg_n(OH)$(Tx) was reduced in $H_2$ (10 mL/min) at 110–190 °C for 3 h to obtain the $Cu_xC$-containing catalyst, which is denoted as $Cu_{10-n}Mg_n(OH)$(Tx-Ry), where y represents the reduction temperature.

### 2.4 Catalyst Characterization

All of the catalysts for characterization were passivated in an 0.50 vol% $O_2/N_2$ flow (10 mL·min$^{-1}$) at ambient temperature for at least 2 h before exposure to air.

X-ray diffraction (XRD) patterns were acquired on a Rigaku SmartLab diffractometer with Cu-Kα radiation source (λ = 0.154 nm) at 200 mA and 45 kV. The XRD patterns were collected in the range of 20–80° with a scanning speed of 8°/min.

Surface morphology was observed by means of scanning electron microscopy (SEM) on an SU8220 instrument with a test voltage of 5.0 kV. Transmission electron microscopy (TEM) images were taken on an FEI Tecnai G2 F30 model with an accelerating voltage of 300 kV.

X-ray photoelectron spectroscopy (XPS) measurement was conducted on an Escalab 250 X-ray photoelectron spectrometer equipped with Al-Kα as the excitation source (1486.6 eV). The binding energy was calibrated using the binding energy of C 1 s at 284.6 eV.

The adsorption/desorption isotherms of nitrogen were measured on a Micromeritics Tristar II 3020 instrument at -196 °C. The specific surface area was calculated from the isotherms according to Brunauer–Emmett–Teller (BET) equation. Thermal gravimetric analysis and differential scanning calorimetry (TG-DSC) were carried out on an instrument (SDT Q600, TA) in a $N_2$ flow (50 mL/min) from room temperature to 500 °C at 3 °C/min.

Hydrogen temperature-programmed reduction ($H_2$-TPR) was carried out on a Chembet-3000 analyzer equipped with a TCD. The sample (0.2 g) was reduced in a stream of $H_2$-containing gas (10.0% $H_2$ in Ar, 50 mL/min) at 10 °C/min up to 600 °C.

### 2.5 Catalytic Performance

The catalytic performance in selective hydrogenation of acetylene was conducted in a tubular quartz fixed-bed reactor. In a typical run, 0.1 g $Cu_{10-n}Mg_n(OH)$ precursor was mixed with quartz sand (0.6 g, 40–80 mesh), and then charged into the middle of the quartz tube reactor (inner diameter: 10 mm). The catalyst bed in the quartz reactor was placed in the constant temperature zone of a tubular electric furnace. $Cu_{10-n}Mg_n(OH)$(Tx-Ry) catalyst was prepared by thermal treatment with $C_2H_2$/Ar gas followed by $H_2$ reduction. Then, the reaction gas (0.8% $CH_4$, 0.5% $C_2H_2$, and 98.7% $C_2H_4$) at 10 mL/min and $H_2$ gas at 1.0 mL/min were fed into the reactor. $CH_4$ was used as the internal standard for gas chromatographic analysis. The outlet gas was analyzed by an online chromatography (Panna A60), equipped with a flame ionization detector and an Agilent HP-AL/S capillary column (30 m × 0.535 mm × 15.00 μm). In addition to ethylene and ethane, a small amount of $C_4^=$ olefins, including trans-2-butene, 1-butylene, cis-2-butene, and 1,3-butadiene, were detected. No green oil was observed downstream of the quartz tube even in the 100-h run.

In the presence of large excess ethylene in the gas feed, it is difficult to accurately measure the selectivity of ethylene. Therefore, the selectivity to undesired ethane was used to determine the selectivity performance of the catalyst, a measure of ethylene gain or loss. The conversion of acetylene and the selectivities to ethane and $C_4^=$ were calculated as follows:

$$C_2H_2\text{conversion}(\%)=\frac{[C_2H_2]_{\text{inlet}}-[C_2H_2]_{\text{outlet}}}{[C_2H_2]_{\text{inlet}}}\times 100 \quad (1)$$

$$C_2H_6\text{selectivity}(\%)=\frac{[C_2H_6]_{\text{outlet}}}{[C_2H_2]_{\text{inlet}}-[C_2H_2]_{\text{outlet}}}\times 100 \quad (2)$$

$$C_4^{=}\text{selectivity}(\%)=\frac{2\times[C4=]_{\text{outlet}}}{[C_2H_2]_{\text{inlet}}-[C_2H_2]_{\text{outlet}}}\times 10 \quad (3)$$

where $[C_2H_2]_{inlet}$ and $[C_2H_2]_{outlet}$ were the mole concentrations of acetylene in the feed and in the effluent, respectively. $[C_2H_6]_{outlet}$ and $[C_4^=]_{outlet}$ were the mole concentrations of ethane and that of total $C_4^=$ olefins, respectively, in the outlet.

In order to accurately determine the selectivity to ethylene, a gas feed of acetylene in $N_2$ (0.5% $C_2H_2$/99.5% $N_2$) was used. The selectivity to ethylene was determined by

$$C_2H_4\text{selectivity}(\%)=\frac{[C_2H_4]_{outlet}}{[C_2H_2]_{inlet}-[C_2H_2]_{outlet}}\times 100 \quad (4)$$

where $[C_2H_4]_{outlet}$ was the mole concentration of ethylene in the effluent.

## 3 Results and Discussion

To investigate the effect of $Mg(OH)_2$ addition on the structure and morphology of the $Cu(OH)_2$ precursor, XRD measurement was conducted, as shown in Fig. 1. In the XRD patterns of $Cu_{10\text{-}n}Mg_n(OH)$, the diffraction peaks at $2\theta = 23.8$, 34.1, 35.9, 38.0, 38.2, 39.8, and 53.2° corresponded to the (021), (002), (111), (041), (022), (130), and (150) planes of $Cu(OH)_2$ (PDF 13–0420), respectively. It is indicated that the intensity of diffraction peaks ascribed to $Cu(OH)_2$ was decreased as the amount of $Mg(OH)_2$ was increased, indicating reduced crystalline size and lower crystallinity of $Cu(OH)_2$ phase. No distinctive diffraction peaks of $Mg(OH)_2$ species were detected in the patterns of all the samples, suggesting that the size of $Mg(OH)_2$ was below the detection limit.

Figure 2a and b illustrate the SEM images of $Cu(OH)_2$ and $Cu_7Mg_3(OH)$, respectively. It is demonstrated that the $Cu(OH)_2$ was in bundles of nanowires, whereas the morphology of $Cu_7Mg_3(OH)$ became a mixture of shorter nanowires and nanosheets, indicating that the introduction of $Mg(OH)_2$ significantly changed the morphology of the obtained catalyst precursor. In the HRTEM images of $Cu_7Mg_3(OH)$ (Fig. S1), the lattice spacings of 0.250 and 0.225 nm corresponded to the (111) and (130) planes of $Cu(OH)_2$, respectively, whereas that of 0.273 nm corresponded to the (100) plane of $Mg(OH)_2$. It is shown that $Cu_7Mg_3(OH)$ was composed of $Cu(OH)_2$ and $Mg(OH)_2$ while the introduction of $Mg(OH)_2$ facilitated the dispersion of $Cu(OH)_2$.

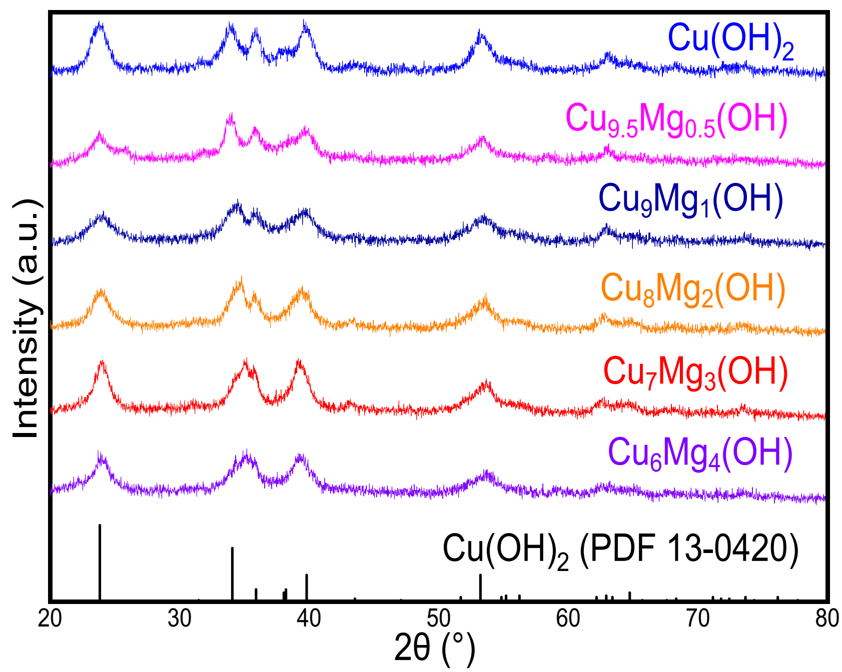


**Fig. 1** XRD patterns of $Cu_{10\text{-}n}Mg_n(OH)$ precursors

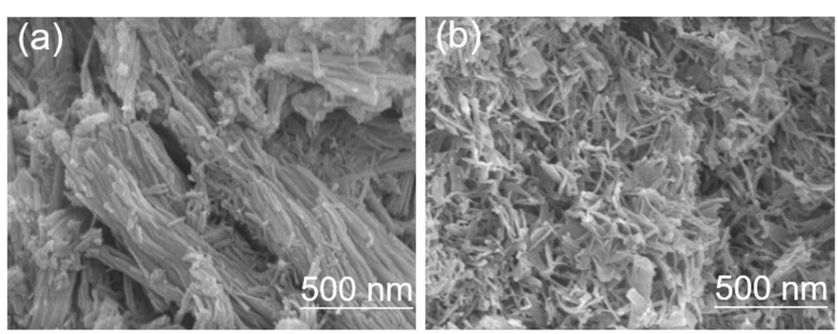


**Fig. 2** SEM images of (**a**) $Cu(OH)_2$ and (**b**) $Cu_7Mg_3(OH)$

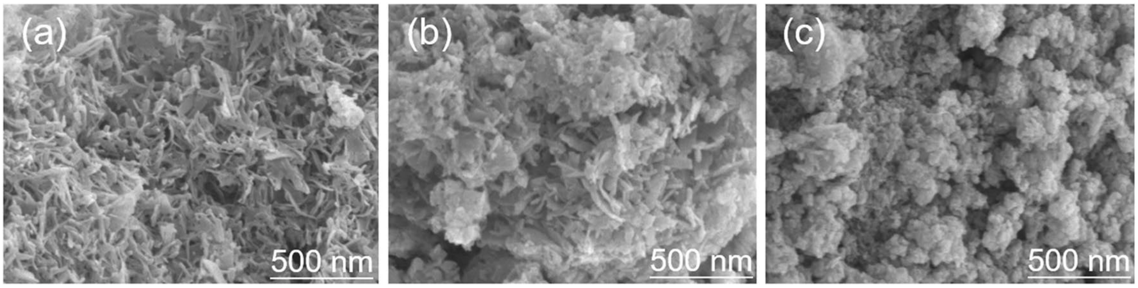


**Fig. 3** SEM images of (**a**) $Cu_7Mg_3(OH)$, (**b**) $Cu_7Mg_3(OH)$(T120) and (**c**) $Cu_7Mg_3(OH)$(T120-R150)

Figure 3 presents the SEM images of $Cu_7Mg_3(OH)$, after thermal treatment with $C_2H_2$/Ar at 120 °C, and after subsequent $H_2$ reduction at 150 °C. It is displayed that $Cu_7Mg_3(OH)$ was in nanosheets, and the nanosheets were covered with cauliflower-shaped materials after the thermal treatment with $C_2H_2$/Ar at 120 °C. When $Cu_7Mg_3(OH)$(T120) was reduced in $H_2$ at 150 °C, the cauliflower shapes shrank in $Cu_7Mg_3(OH)$(T120-R150). It implies that the reaction of $Cu(OH)_2$ with acetylene occurred in the thermal treatment, producing fabrics on the surface. The subsequent hydrogen reduction did not change the morphology significantly but reduced the length of the hydrocarbon fabrics.

As shown in Fig. 4a, after the thermal treatment with acetylene-containing gas, the XRD pattern of $Cu_7Mg_3(OH)$(T120) remained similar to that of $Cu_7Mg_3(OH)$, suggesting that the reaction with acetylene took place on the external surface of the precursor. The weaker diffraction peaks characteristic of $Cu(OH)_2$ in the XRD pattern of $Cu_7Mg_3(OH)$(T120) than $Cu_7Mg_3(OH)$ was attributed to reduced particle size of the precursor and to the presence of amorphous hydrocarbon fabrics on the external surface. In the XRD pattern of $Cu_7Mg_3(OH)$(T120-R150) (Fig. 4b), the intense peaks at $2\theta = 43.3$, 50.4, and 74.1° were ascribed to the (111), (200), and (220) planes of metal Cu (PDF 04–0836), indicating that the core of the precursor was reduced to generate metal Cu particles at temperature as low as 150 °C. An additional weak peak at $2\theta = 37.2°$ was indicative of the formation $Cu_xC$ crystal [41–47]. The intensity of this characteristic peak attributed to $Cu_xC$ in $Cu_7Mg_3(OH)$(T120-R150) was lower than that of $Cu(OH)_2$(T120-R150) [43], indicating that the crystalline size of $Cu_xC$ derived from $Cu_7Mg_3(OH)$ was smaller, probably because of decreased size of $Cu(OH)_2$ particles in the precursor.

In the HRTEM image of $Cu_7Mg_3(OH)$(T120-R150) (Fig. 5), three kinds of crystallites were observed. The lattice spacing of 0.208 nm corresponded to the (111) plane of Cu, whereas that of 0.273 nm corresponded to the (100) plane of $Mg(OH)_2$. It implies that Mg species existed in the form of $Mg(OH)_2$ instead of MgO in $Cu_7Mg_3(OH)$(T120-R150), which was in agreement with the TG-DSC measurement of $Mg(OH)_2$ (Fig. S2).The lattice spacing of 0.240 nm corresponded to that of $Cu_xC$ crystallite [41]. Fig. S3 shows the EDS elementary mapping analysis of $Cu_7Mg_3(OH)$(T120-R150). It is demonstrated that Cu species, $Mg(OH)_2$ and C species were homogeneously distributed in $Cu_7Mg_3(OH)$(T120-R150). Moreover, the specific surface areas, calculated from the $N_2$ adsorption–desorption isotherms (Fig. S4) using Brunauer–Emmett–Teller (BET) methods, indicated that, after treatment with acetylene-containing gas and subsequent hydrogen reduction, the surface area increased from 84, to 117, and to 123 $m^2/g$, respectively (Table S1). The significant increment after thermal

**Fig. 4** (**a**) XRD patterns of $Cu_7Mg_3(OH)$(T120-R150), $Cu_7Mg_3(OH)$(T120) and $Cu_7Mg_3(OH)$ (**b**) XRD pattern of $Cu_7Mg_3(OH)$(T120-R150)

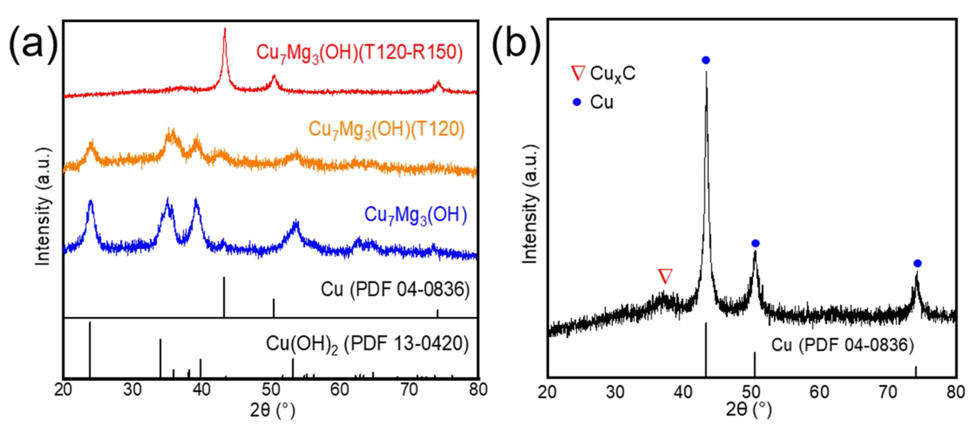

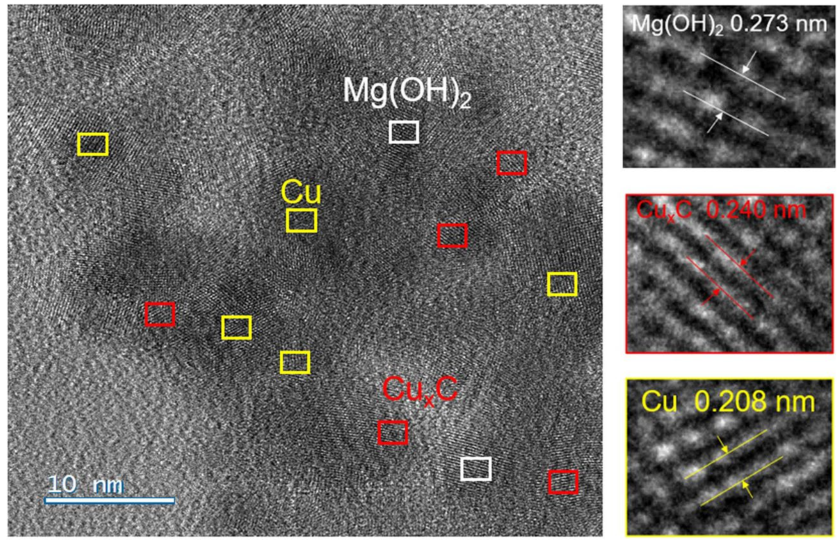


**Fig. 5** HRTEM image of $Cu_7Mg_3(OH)$(T120-R150)

treatment with acetylene might be due to the formation of external fabrics and amorphous carbonaceous materials [41]. Therefore, it is concluded that $Cu_7Mg_3(OH)$(T120-R150) was composed of $Cu_xC$, Cu and $Mg(OH)_2$ nanoparticles, which were embedded in the matrix of amorphous carbonaceous materials.

Figure 6 illustrates the XPS spectra of $Cu_7Mg_3(OH)$(T120-R150). The absence of a satellite peak at ~ 943 eV in the Cu $2p_{3/2}$ spectrum suggests that there was no $Cu^{2+}$ species [49], corroborating that the surface $Cu(OH)_2$ was transformed by reacting with $C_2H_2$ followed by hydrogen reduction (Fig. 6a). The major peak was centered at binding energy of 932.6 eV (Fig. 6a), which fell between that of $Cu^{2+}$ and that $Cu^0/Cu^+$. Since it is not possible to distinguish $Cu^0$ and $Cu^+$ in the Cu $2p_{3/2}$ spectrum, Cu LMM spectrum of $Cu_7Mg_3(OH)$(T120-R150) was measured, and is presented in Fig. 6b. It is indicated that the peak was centered at 917.7 eV, which was between that of $Cu^0$ (918.7 eV) [50] and that of $Cu^+$ (916.8 eV) [51]. It implies that the major contribution to this peak came from partially positive

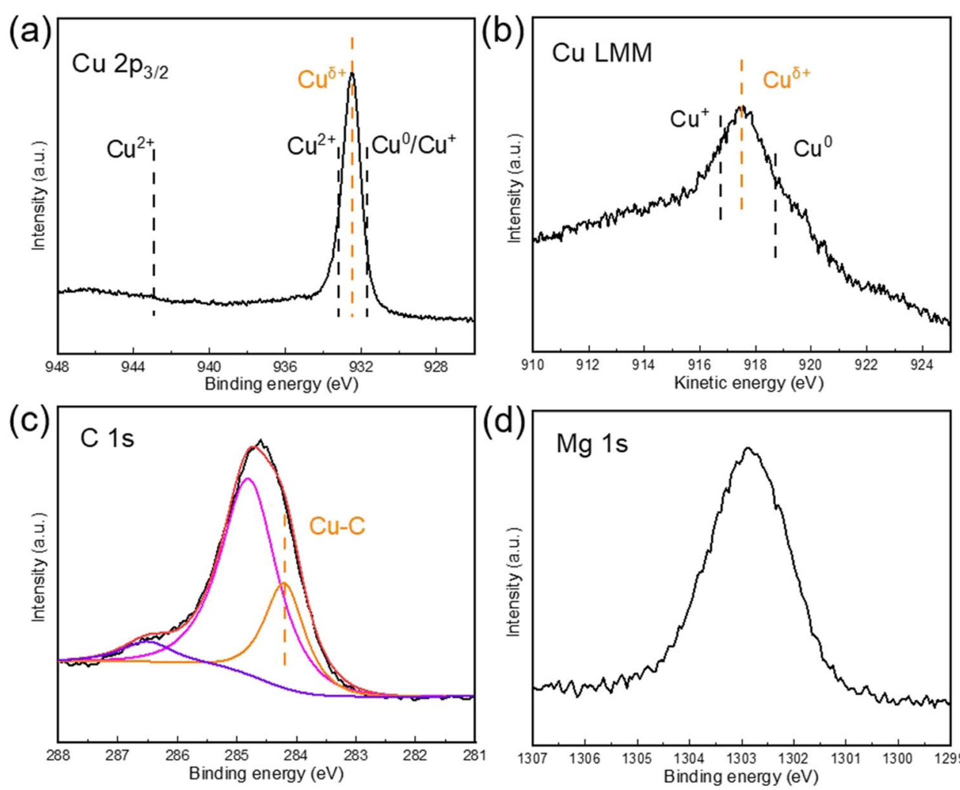


**Fig. 6** XPS spectra of $Cu_7Mg_3(OH)$(T120-R150). (**a**) Cu $2p_{3/2}$, (**b**) Cu LMM spectrum, (**c**) C 1 s, and (**d**) Mg 1 s

species of Cu ($Cu^{\delta+}$), which is characteristic of interstitial copper carbide ($Cu_xC$) [41, 52]. In the C 1 s spectrum of $Cu_7Mg_3(OH)$(T120-R150) (Fig. 6c), the large peak was tentatively deconvoluted into three peaks at binding energies of 284.9, 286.5, and 284.2 eV. The peak at 284.9 was attributed to the C–C bond [52], whereas the shoulder peak at 286.5 eV corresponded to the C–OH species [53]. Kim et al. [52] concluded that the simultaneous appearance of the two peaks at 932.6 eV in the Cu $2p_{3/2}$ spectrum and at 284.2 eV in the C 1 s spectrum was due to the formation of copper carbide. In the XPS spectrum of Mg 1 s (Fig. 6d), the peak at binding energy of 1302.8 eV was attributed to $Mg(OH)_2$ in $Cu_7Mg_3(OH)$(T120-R150) [54], which is in agreement with the HRTEM observation (Fig. 5).

In our previous investigation [43], the catalysts derived from $Cu(OH)_2$ showed an excellent performance in acetylene selective hydrogenation. It was found that $Cu_xC$ served as the catalytic site for hydrogen dissociation whereas acetylene hydrogenation mainly occurred on Cu site. The addition of $Mg(OH)_2$ may affect the fraction of $Cu_xC$ in the preparation. Therefore, the effect of the composition of Cu and Mg in the precursor on acetylene conversion and ethane selectivity was investigated. Figure 7 compares the catalytic performances of catalysts prepared from various $Cu_{10-n}Mg_n(OH)$ (n = 0.5, 1, 2, 3, 4) precursors, which were treated with acetylene-containing gas at 120 ℃ for 2 h and then reduced in $H_2$ at 150 °C for 3 h. With the addition of $Mg(OH)_2$, all $Cu_{10-n}Mg_n(OH)$(T120-R150) (n = 0.5, 1, 2, 3, 4) showed higher hydrogenation activity than $Cu(OH)_2$(T120-R150) at 100 ℃, probably due to increased amount of $Cu_xC$ crystallites in $Cu_{10-n}Mg_n(OH)$(T120-R150). $Cu_9Mg_1(OH)$(T120-R150) exhibited the highest hydrogenation activity, implying that more $Cu_xC$ crystallites were present. However, a considerably higher amount of unwanted ethane was produced on $Cu_9Mg_1(OH)$(T120-R150), leading to a marked ethylene loss. For $Cu_8Mg_2(OH)$(T120-R150), acetylene conversion decreased slightly whereas the selectivity to ethane was reduced significantly. $Cu_7Mg_3(OH)$(T120-R150) showed the best performance with extremely high hydrogenation activity and an ethylene gain (ethane selectivity < 30%). The outstanding catalytic performance of $Cu_7Mg_3(OH)$(T120-R150) might be related with the optimal composition of $Cu_xC$ and Cu phases. Therefore, $Cu_7Mg_3(OH)$ was chosen the catalyst precursor in the subsequent investigation.

The influence of acetylene treatment temperature on the catalytic performance of $Cu_7Mg_3(OH)$-derived catalysts in acetylene selective hydrogenation is shown in Fig. 8. The $Cu_7Mg_3(OH)$ precursor was treated with acetylene-containing gas at various temperature in the range of 100–180 ℃ for 2 h and then reduced in $H_2$ at 150 °C for 3 h. Acetylene conversion increased at first and then decreased with the treatment temperature. On one hand, higher acetylene treatment temperature might enhance the decomposition of the in situ generated copper acetylide ($CuC_2$). On the other hand, less amount of intermediate $CuC_2$ was formed at lower treatment temperatures, leading to less formation of $Cu_xC$ active phase in the subsequent hydrogen reduction.

The influence of acetylene treatment time on the catalytic performance is shown in Fig. 9. The acetylene conversion reached nearly 100% when the precursor was treated at 120 ℃ for 2 or 3 h. However, at longer treatment time (4 h), the conversion decreased, probably because the decomposition of intermediate $CuC_2$ was enhanced at a long thermal

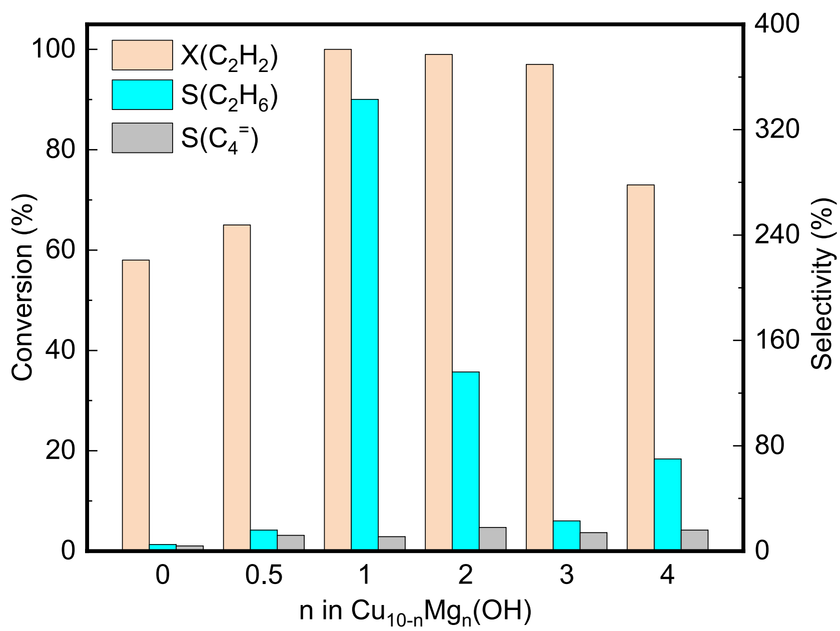


**Fig. 7** Effect of $Mg(OH)_2$ amount on the acetylene selective hydrogenation performance catalyzed by $Cu_{10-n}Mg_n(OH)$(T120-R150) at 100 °C

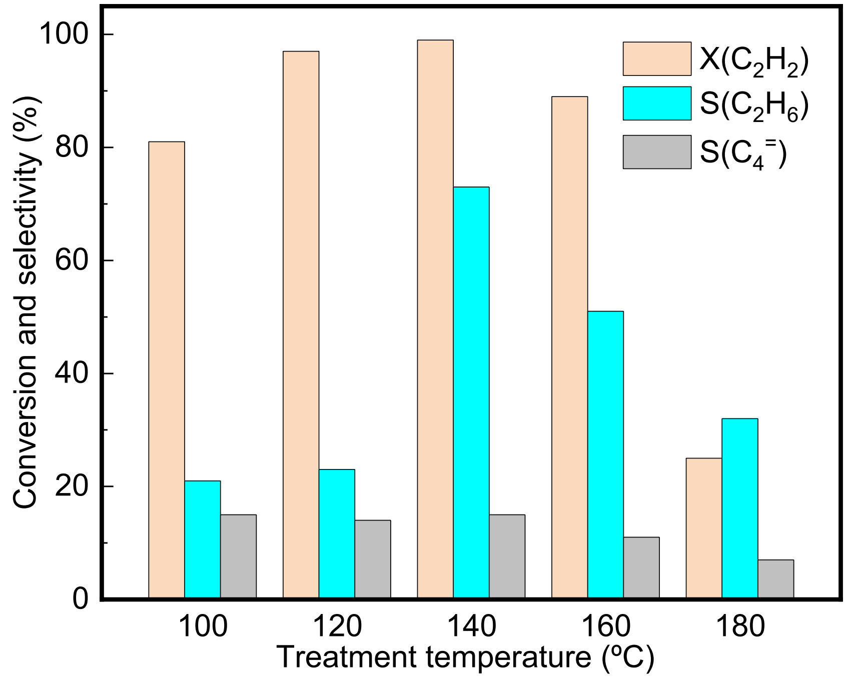


**Fig. 8** Effect of acetylene treatment temperature on the acetylene selective hydrogenation performance catalyzed by $Cu_7Mg_3$(OH)(Tx-R150) at 100 °C

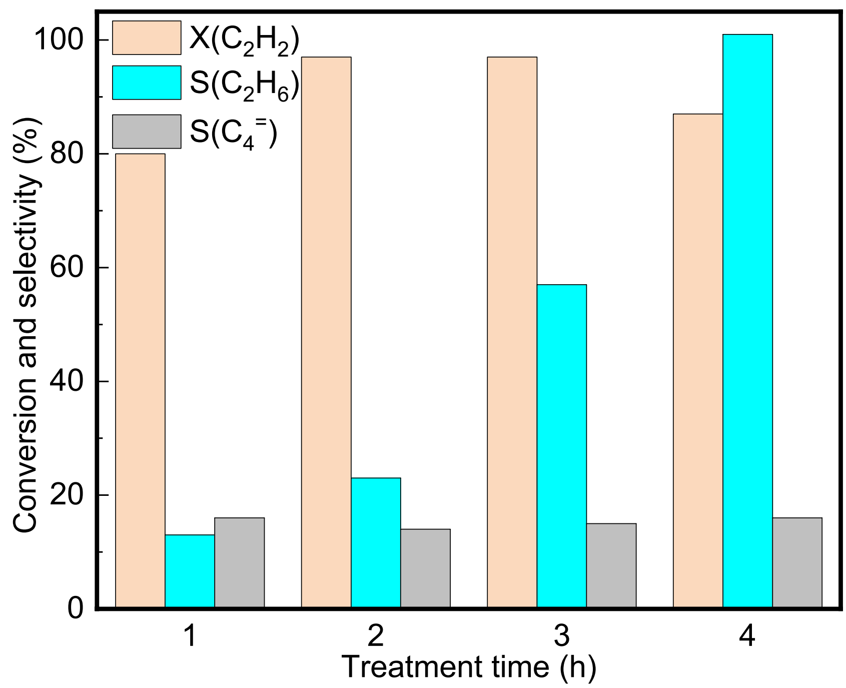


**Fig. 9** Effect of acetylene treatment time on the acetylene selective hydrogenation performance catalyzed by $Cu_7Mg_3$(OH)(T120-R150) at 100 °C

treatment time, which is in agreement with our previous results [43].

Under the optimal treatment conditions (120 °C for 2 h), the influence of hydrogen reduction temperature on the catalytic performance in selective hydrogenation of acetylene was investigated (Fig. 10). $Cu_7Mg_3$(OH)(T120) was reduced in $H_2$ at various temperatures in the range of 110–190 °C for 3 h. The catalysts prepared by hydrogen reduction in the temperature range of 130 to 170 °C exhibited significantly high activity for acetylene hydrogenation with nearly 100% acetylene conversion at 100 °C, while the catalyst obtained by hydrogen reduction at 190 °C showed a slightly lower acetylene conversion (91%) under the same conditions. Although the rate of $CuC_2$ reduction to yield $Cu_xC$ was high at higher reduction temperatures, the parallel decomposition of $CuC_2$ was enhanced as well, resulting in less production of $Cu_xC$. Interestingly, the catalysts prepared by hydrogen reduction

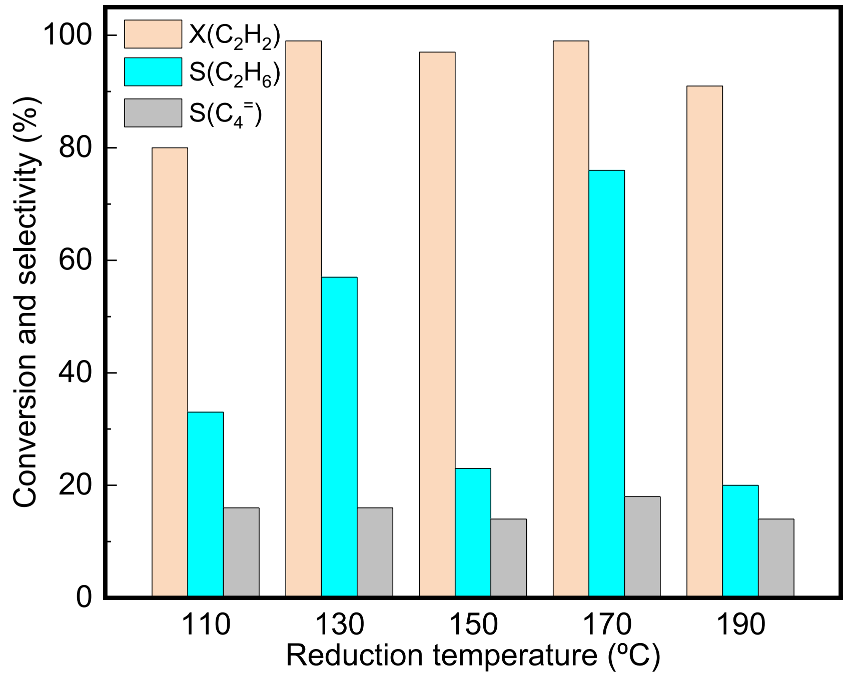


**Fig. 10** Effect of reduction temperature on the acetylene selective hydrogenation performance catalyzed by $Cu_7Mg_3(OH)$ (T120-Ry) at 100 °C

**Table 1** Product selectivity in hydrogenation of acetylene in large excess of ethylene catalyzed by $Cu(OH)_2$(T120-R150) and $Cu_7Mg_3(OH)$ (T120-R150)

| Catalysts | Reaction temperature /℃ | Acetylene conversion /% | Product selectivity /% | |
|---|---|---|---|---|
| | | | $C_2H_6$ | $C_4^=$ |
| $Cu(OH)_2$ (T120-R150) | 100 | 63 | 5 | 3 |
| | 110 | 100 | 19 | 16 |
| | 120 | 100 | 42 | 15 |
| $Cu_7Mg_3(OH)$ (T120-R150) | 90 | 10 | 3 | 0 |
| | 100 | 97 | 23 | 14 |
| | 110 | 100 | 98 | 10 |

at 130 and 170 ℃ both showed full acetylene conversion, probably due to a balanced reduction and decomposition of $CuC_2$ in the catalyst preparation. Nevertheless, both catalysts showed high selectivity to undesired ethane, and, as a consequence, the optimal reduction temperature was chosen to be 150 °C.

Table 1 presents acetylene conversion and selectivities to ethane and $C_4^=$ as a function of reaction temperature in hydrogenation of acetylene in excess ethylene over $Cu(OH)_2$(T120-R150) and $Cu_7Mg_3(OH)$(T120-R150). It can be seen that both catalysts gave low selectivities to ethane and $C_4^=$ when acetylene was not completely converted at low temperatures. However, when acetylene was 100%, large amounts of ethane and $C_4^=$ were yielded. When the reaction temperature was further increased, both catalysts showed reduced selectivity to $C_4^=$ at 100% acetylene conversion because high temperature led to enhanced hydrogen dissociation, thus increasing ethane selectivity while decreasing the selectivity to $C_4^=$, in agreement with the published results [55–57]. Table S2 compares the results in hydrogenation of acetylene in nitrogen (0.5% $C_2H_2$/99.5% $N_2$) over $Cu(OH)_2$(T120-R150) and $Cu_7Mg_3(OH)$(T120-R150). Similarly, high temperature was unfavorable to the production of $C_4^=$ at complete conversion of acetylene. Additionally, $Cu_7Mg_3(OH)$ (T120-R150) yielded less $C_4^=$ than $Cu(OH)_2$(T120-R150) in the investigated temperature range, probably because the presence of $Mg(OH)_2$ in $Cu_7Mg_3(OH)$(T120-R150) might suppress significantly the production of $C_4^=$ and undesired oligomers [56, 58, 59].

Figure 11 displays the dependence of acetylene conversion and ethane selectivity on $H_2/C_2H_2$ ratio in acetylene selective hydrogenation catalyzed by $Cu_7Mg_3(OH)$ (T120-R150) at 100 °C and atmospheric pressure. In the range of 14–30, the acetylene conversion and ethane selectivity increased gradually with $H_2/C_2H_2$ ratio. At $H_2/C_2H_2$ ratio of 22, complete acetylene conversion was obtained with an ethane selectivity of 24%. In the range of 24–30, the ethane selectivity markedly increased with $H_2/C_2H_2$ ratio, causing an ethylene loss. Compared with $Cu(OH)_2$(T120-R150) [43], $Cu_7Mg_3(OH)$(T120-R150) exhibited higher hydrogenation activity, with complete acetylene removal in ethylene stream at 100 ℃ and atmospheric pressure.

Copper-based catalysts are known to deactivate quickly due to the formation of green oil, which was accumulated on the catalyst surface [55]. In our investigation, there was no green oil downstream of the quartz tube in the course of a 100-h reaction. The

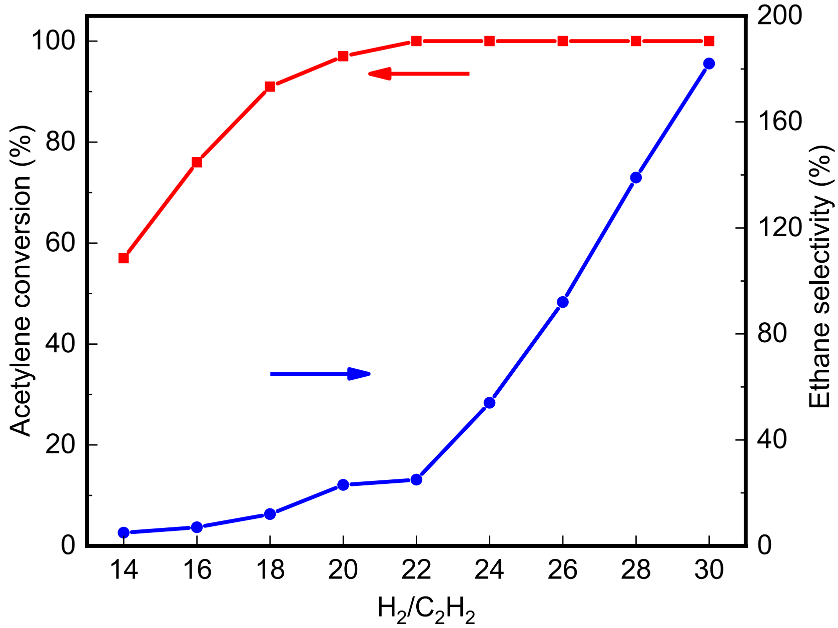


**Fig. 11** Effect of $H_2/C_2H_2$ ratio on the acetylene selective hydrogenation performance catalyzed by $Cu_7Mg_3(OH)$(T120-R150) at 100 °C and atmospheric pressure

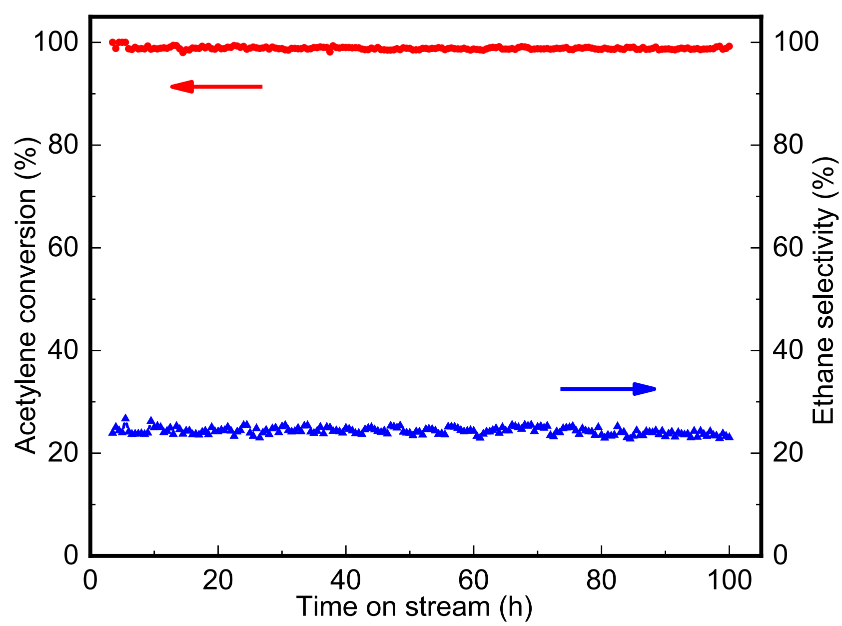


**Fig. 12** Variation of acetylene selective hydrogenation performance with time on stream catalyzed by $Cu_7Mg_3(OH)$(T120-R150) at 100 °C

variation of acetylene conversion and ethane selectivity with time on stream in selective hydrogenation of acetylene catalyzed by $Cu_7Mg_3(OH)$(T120-R150) are demonstrated in Fig. 12. It is indicated that $Cu_7Mg_3(OH)$(T120-R150) was stable in a 100-h run at 100 °C and atmospheric pressure, achieving complete removal of acetylene in ethylene with low selectivity to undesired ethane (24%). The high stability with an ethylene gain might be attributed to the formation of the porous carbonaceous matrix formed by the decomposition of intermediate $CuC_2$ on the external surface of the catalyst, which suppressed the chain growth of linear hydrocarbons because of steric hindrance [41–45]. Additionally, $Mg(OH)_2$ in $Cu_7Mg_3(OH)$(T120-R150) helped to suppress the production of $C_4^{=}$, among which 1,3-butadiene is considered to be the precursor of green oil.

## 4 Conclusions

In summary, a catalyst for selective hydrogenation of acetylene was prepared from copper and magnesium hydroxides through thermal treatment with acetylene-containing gas followed by hydrogen reduction. The catalyst was composed of $Cu_xC$, Cu, and $Mg(OH)_2$ enwrapped in a porous carbon matrix. Among them, $Cu_xC$ was considered to be the highly active site for hydrogen dissociation, Cu mainly acted as the site for selective hydrogenation of acetylene, and the porous carbon layer helped to block the chain growth of linear hydrocarbons. $Mg(OH)_2$ facilitated the formation of highly dispersed $Cu_xC$ crystallites with enhanced hydrogenation activity, and its basicity was favorable to suppress the formation of $C_4^=$. The prepared catalysts exhibited remarkably high performance with complete acetylene conversion, low ethane selectivity (24%), and high stability in removal of acetylene impurity of ethylene stream at 100 °C and atmospheric pressure in a 100-h run. This work provides a new approach to preparing non-noble catalysts for a variety of hydrogenations under mild conditions.

**Supplementary Information** The online version contains supplementary material available at https://doi.org/10.1007/s10562-024-04686-y.

**Acknowledgements** This work was supported by the National Natural Science Foundation of China (22172015, 21972014, 22172012, and 22202024).

**Author Contributions** The manuscript was written through contributions of all authors. All authors have given approval to the final version of the manuscript.

**Funding** National Natural Science Foundation of China,21972014,22172012,22172015,22202024

## Declarations

**Competing Interest** The authors declare no competing financial interest or personal relationships that could have appeared to influence the work reported in this paper.

## References

1. Huang F, Deng Y, Chen Y, Cai X, Peng M, Jia Z, Ren P, Xiao D, Wen X, Wang N, Liu H, Ma D (2018) Atomically Dispersed Pd on Nanodiamond/Graphene Hybrid for Selective Hydrogenation of Acetylene. J Am Chem Soc 140:13142–13146
2. Chai M, Liu X, Li L, Pei G, Ren Y, Su Y, Cheng H, Wang A, Zhang T (2017) $SiO_2$-Supported Au-Ni Bimetallic Catalyst for the Selective Hydrogenation of Acetylene. Chin J Catal 38:1338–1346
3. Kim SK, Kim C, Lee JH, Kim J, Lee H, Moon SH (2013) Performance of Shape-Controlled Pd Nanoparticles in the Selective Hydrogenation of Acetylene. J Catal 306:146–154
4. Liu H, Chai M, Pei G, Liu X, Li L, Kang L, Wang A, Zhang T (2020) Effect of IB-Metal on $Ni/SiO_2$ Catalyst for Selective Hydrogenation of Acetylene. Chin J Catal 41:1099–1108
5. Rijo B, Lemos F, Fonseca I, Vilelas A (2020) Development of a Model for an Industrial Acetylene Hydrogenation Reactor Using Plant Data - Part I. Chem Eng J 379:122390
6. Pradier CM, Mazina M, Berthier Y, Oudar J (1994) Hydrogenation of acetylene on palladium. J Mol Catal 89:211–220
7. Sárkány A, Beck A, Horváth A, Révay Z, Guczi L (2003) Acetylene Hydrogenation on Sol-derived $Pd/SiO_2$. Appl Catal A: Gen 253:283–292
8. Yang Z, Li Y, Cao Y, Zhao X, Chen W, Zhang J, Qian G, Peng C, Gong X, Duan X (2022) $Al_2O_3$ Microrods Supported Pd Catalysts for Semi-Hydrogenation of Acetylene: Acidic Properties Tuned Reaction Kinetics Behaviors. Chem Eng J 445:136681
9. Cao Y, Ge X, Li Y, Si R, Sui Z, Zhou J, Duan X, Zhou X (2021) Structural and Kinetics Understanding of Support Effects in Pd-Catalyzed Semi-Hydrogenation of Acetylene. Engineering 7:103–110
10. Liu Y, Fu F, McCue A, Jones W, Rao D, Feng J, He Y, Li D (2020) Adsorbate-Induced Structural Evolution of Pd Catalyst for Selective Hydrogenation of Acetylene. ACS Catal 10:15048–15059
11. McCue AJ, Anderson JA (2015) CO Induced Surface Segregation as a Means of Improving Surface Composition and Enhancing Performance of CuPd Bimetallic Catalysts. J Catal 329:538–546
12. Borodziński A, Bond GC (2008) Selective Hydrogenation of Ethyne in Ethene-Rich Streams on Palladium Catalysts, Part 2: Steady-State Kinetics and Effects of Palladium Particle Size, Carbon Monoxide, and Promoters. Catal Rev-Sci Eng 50:379–469
13. Nikolaev SA, Zanaveskin LN, Smirnov VV, Averyanov VA, Zanaveskin KL (2009) Catalytic Hydrogenation of Alkyne and Alkadiene Impurities in Alkenes. Practical and Theoretical Aspects. Russ Chem Rev 78:231–247
14. Bukhtiyarov AV, Panafidin MA, Prosvirin IP, Mashkovsky IS, Markov PV, Rassolov AV, Smirnova NS, Baeva GN, Rameshan C, Rameshan R, Zubavichus YV, Bukhtiyarov VI, Stakheev AY (2022) Boosting the Activity of $PdAg_2/Al_2O_3$ Supported Catalysts towards the Selective Acetylene Hydrogenation by Means of CO-Induced Segregation: A Combined NAP XPS and Mass-Spectrometry Study. Appl Surf Sci 604:154497
15. Afonasenko TN, Temerev VL, Shlyapin DA, Tsyrul'Nikov PG (2019) Liquid-Phase Hydrogenation of Acetylene to Ethylene in a Flow on $Pd/Al_2O_3$ and $Pd-Ga/Al_2O_3$ Catalysts in the Presence of CO. Russ J Appl Chem 92:128–134
16. Wang J, Xu H, Che C, Zhu J, Cheng D (2023) Rational Design of PdAg Catalysts for Acetylene Selective Hydrogenation via Structural Descriptor-Based Screening Strategy. ACS Catal 13:433–444
17. Ma R, He Y, Feng J, Hu Z, Van Tendeloo G, Li D (2019) A Facile Synthesis of Ag@PdAg Core-Shell Architecture for Efficient Purification of Ethene Feedstock. J Catal 369:440–449
18. Chen L, Li X, Ma S, Hu Y, Shang C, Liu Z (2022) Highly Selective Low-Temperature Acetylene Semihydrogenation Guided by Multiscale Machine Learning. ACS Catal 12:14872–14881
19. Li X, Chen L, Shang C, Liu Z (2021) In Situ Surface Structures of PdAg Catalyst and Their Influence on Acetylene Semihydrogenation Revealed by Machine Learning and Experiment. J Am Chem Soc 143:6281–6292
20. Wang Y, Qi Y, Fan M, Wang B, Ling L, Zhang R (2022) $C_2H_2$ Semi-Hydrogenation on the $Pd_xM_y$ Cluster/Graphdiyne Catalysts: Effects of Cluster Composition and Size on the Activity and Selectivity. Green Energy Environ 7:500–511
21. Huang F, Peng M, Chen Y, Cai X, Qin X, Wang N, Xiao D, Jin L, Wang G, Wen X, Liu H, Ma D (2022) Low-Temperature Acetylene Semi-Hydrogenation over the $Pd_1$-$Cu_1$ Dual-Atom Catalyst. J Am Chem Soc 144:18485–18493
22. Yang T, Feng Y, Ma R, Li Q, Yan H, Liu Y, He Y, Miller JT, Li D (2021) Improvement of Selectivity in Acetylene Hydrogenation with Comparable Activity over Ordered PdCu Catalysts Induced by Post-treatment. ACS Appl Mater Inter 13:706–716
23. Yuan Z, Liu L, Ru W, Zhou D, Kuang Y, Feng J, Liu B, Sun X (2022) 3D Printed Hierarchical Spinet Monolithic Catalysts for Highly Efficient Semi-Hydrogenation of Acetylene. Nano Res 15:6010–6018

24. Qin C, Guo Q, Guo J, Chen P (2021) Atomically Dispersed Pd Atoms on a Simple MgO Support with an Ultralow Loading for Selective Hydrogenation of Acetylene to Ethylene. Chem-Asian J 16:1225–1228
25. Guo Y, Qi H, Su Y, Jiang Q, Cui Y, Li L, Qiao B (2021) High Performance of Single-Atom Catalyst $Pd_1/MgO$ for Semi-Hydrogenation of Acetylene to Ethylene in Excess Ethylene. ChemNanoMat 7:526–529
26. Lomonosov V, Wayman TMR, Hopper ER, Ivanov YP, Divitini G, Ringe E (2023) Plasmonic Magnesium Nanoparticles Decorated with Palladium Catalyze Thermal and Light-Driven Hydrogenation of Acetylene. Nanoscale 15:7420–7429
27. Dasgupta A, He H, Gong R, Shang S, Zimmerer EK, Meyer RJ, Liu Z, Janik MJ, Rioux RM (2022) Atomic Control of Active-Site Ensembles in Ordered Alloys to Enhance Hydrogenation Selectivity. Nat Chem 14:523–529
28. Wang S, Zhu J, Si J, Zhao G, Liu Y, Lu Y (2020) High-Performance Pd/Brass-fiber Catalyst for Selective Hydrogenation of Acetylene : Effect of Calcination-Assisted Endogenous Growth of $ZnO\text{-}CuO_x$ on Brass-Fiber. J Catal 382:295–304
29. Niu Y, Wang Y, Chen J, Li S, Huang X, Willinger M, Zhang W, Liu Y, Zhang B (2022) Patterning the Consecutive $Pd_3$ to $Pd_1$ on $Pd_2Ga$ Surface via Temperature-Promoted Reactive Metal-Support Interaction. Sci Adv 8: eabq5751
30. He Y, Liang L, Liu Y, Feng J, Ma C, Li D (2014) Partial hydrogenation of acetylene using highly stable dispersed bimetallic $Pd\text{-}Ga/MgO\text{-}Al_2O_3$ catalyst. J Catal 309:166–173
31. Menezes WG, Altmann L, Zielasek V, Thiel K, Bäumer M (2013) Bimetallic Co-Pd Catalysts: Study of Preparation Methods and Their Influence on the Selective Hydrogenation of Acetylene. J Catal 300:125–135
32. Yurpalova DV, Afonasenko TN, Prosvirin IP, Bukhtiyarov AV, Panafidin MA, Vinokurov ZS, Trenikhin MV, Gerasimov EY, Gulyaeva TI, Kovtunova LM, Shlyapin DA (2023) Selective Hydrogenation of Acetylene over Pd-Co/C Catalysts: The Modifying Effect of Cobalt. Catalysts 13:739
33. Cao Y, Sui Z, Zhu Y, Zhou X, Chen D (2017) Selective Hydrogenation of Acetylene over $Pd\text{-}In/Al_2O_3$ Catalyst: Promotional Effect of Indium and Composition-Dependent Performance. ACS Catal 7:7835–7846
34. Feng Q, Zhao S, Wang Y, Dong J, Chen W, He D, Wang D, Yang J, Zhu Y, Zhu H, Gu L, Li Z, Liu Y, Yu R, Li J, Li Y (2017) Isolated Single-Atom Pd Sites in Intermetallic Nanostructures: High Catalytic Selectivity for Semihydrogenation of Alkynes. J Am Chem Soc 139:7294–7301
35. Wang L, Li F, Chen Y, Chen J (2019) Selective Hydrogenation of Acetylene on $SiO_2$-Supported Ni-Ga Alloy and Intermetallic Compound. J Energy Chem 29:40–49
36. Cao Y, Zhang H, Ji S, Sui Z, Jiang Z, Wang D, Zaera F, Zhou X, Duan X, Li Y (2020) Adsorption Site Regulation to Guide Atomic Design of Ni-Ga Catalysts for Acetylene Semi-Hydrogenation. Angew Chem Int Ed 59:11647–11652
37. Fu F, Liu Y, Li Y, Fu B, Zheng L, Feng J, Li D (2021) Interfacial Bifunctional Effect Promoted Non-Noble $Cu/Fe_yMgO_x$ Catalysts for Selective Hydrogenation of Acetylene. ACS Catal 11:11117–11128
38. Shi X, Lin Y, Huang L, Sun Z, Yang Y, Zhou X, Vovk E, Liu X, Huang X, Sun M, Wei S, Lu J (2020) Copper Catalysts in Semihydrogenation of Acetylene : From Single Atoms to Nanoparticles. ACS Catal 10:3495–3504
39. Huang F, Peng M, Liu H, Ma D (2023) Atomically Dispersed Metals on Nanodiamond-Derived Hybrid Materials for Heterogeneous Catalysis. ACC Mater Res 4:223–236
40. Huang F, Deng Y, Chen Y, Cai X, Peng M, Jia Z, Xie J, Xiao D, Wen X, Wang N, Jiang Z, Liu H, Ma D (2019) Anchoring $Cu_1$ Species over Nanodiamond-Graphene for Semi-Hydrogenation of Acetylene. Nat Commun 10:4431
41. Lu C, Wang Y, Zhang R, Wang B, Wang A (2020) Preparation of an Unsupported Copper-Based Catalyst for Selective Hydrogenation of Acetylene from $Cu_2O$ Nanocubes. ACS Appl Mater Inter 12:46027–46036
42. Lu C, Zeng A, Wang Y, Wang A (2021) High-Performance Catalysts Derived from Cupric Subcarbonate for Selective Hydrogenation of Acetylene in an Ethylene Stream. Eur J Inorg Chem 2021:997–1004
43. Lu C, Zeng A, Wang Y, Wang A (2021) Copper-Based Catalysts for Selective Hydrogenation of Acetylene Derived from $Cu(OH)_2$. ACS Omega 6:3363–3371
44. Zeng A, Lu C, Xu B, Wang A, Liu Y, Sun Z, Wang Y (2023) A Highly Active Catalyst Derived from CuO Particles for Selective Hydrogenation of Acetylene in Large Excess Ethylene. Phys Chem Chem Phys 25:14598–14605
45. Lu C, Zeng A, Wang Y, Wang A (2022) Enhanced Hydrogenation Activity over a Zn-Modified Cu-Based Catalyst in Acetylene Hydrogenation. Ind Eng Chem Res 61:18696–18702
46. Yao Y, Yu Z, Lu C, Sun F, Wang Y, Sun Z, Liu Y, Wang A (2022) Highly Efficient Cu-Based Catalysts for Selective Hydrogenation of Furfural: A Key Role of Copper Carbide. Renew Energy 197:69–78
47. Liu S, Yu Z, Lu C, Wang Y, Sun F, Sun Z, Liu Y, Shi C, Wang A (2023) Copper Carbide Composite Catalyst for Hydrogenolysis of Glycerol to 1,2-Propanediol. Fuel 334:126763
48. Zhao Z, Zhao J, Chang X, Zha S, Zeng L, Gong J (2019) Competition of C-C Bond Formation and C-H Bond Formation for Acetylene Hydrogenation on Transition Metals: A Density Functional Theory Study. AIChE J 65:1059–1066
49. Bao H, Zhang W, Hua Q, Jiang Z, Yang J, Huang W (2011) Crystal-Plane-Controlled Surface Restructuring and Catalytic Performance of Oxide Nanocrystals. Angew Chem Int Ed 50:12294–12298
50. Fox EB, Velu S, Engelhard MH, Chin Y, Miller JT, Kropf J, Song C (2008) Characterization of $CeO_2$-Supported Cu-Pd Bimetallic Catalyst for the Oxygen-Assisted Water-Gas Shift Reaction. J Catal 260:358–370
51. Wang J, Li C, Zhu Y, Boscoboinik JA, Zhou G (2022) In Situ Monitoring of $H_2$-Induced Nonstoichiometry in $Cu_2O$. J Phys Chem Lett 13:5597–5604
52. Kim S, Son Y, Choi K, Kim S, Son Y, Park J, Lee JH, Jang J (2018) Highly Active Bifunctional Electrocatalysts for Oxygen Evolution and Reduction in Zn-Air Batteries. Chemsuschem 11:4203–4208
53. Martínez MT, Callejas MA, Benito AM, Cochet M, Seeger T, Ansón A, Schreiber J, Gordon C, Marhic C, Chauvet O, Fierro JLG, Maser WK (2003) Sensitivity of Single Wall Carbon Nanotubes to Oxidative Processing: Structural Modification, Intercalation and Functionalisation. Carbon 41:2247–2256
54. Zhang F, Zhang C, Zeng R, Song L, Guo L, Huang X (2016) Corrosion Resistance of the Superhydrophobic $Mg(OH)_2$/Mg-Al Layered Double Hydroxide Coatings on Magnesium Alloys. Metals 6:85
55. Bridier B, Pérez-Ramírez J (2010) Cooperative Effects in Ternary Cu-Ni-Fe Catalysts Lead to Enhanced Alkene Selectivity in Alkyne Hydrogenation. J Am Chem Soc 132:4321–4327
56. Bridier B, López N, Pérez-Ramírez J (2010) Partial Hydrogenation of Propyne over Copper-Based Catalysts and Comparison with Nickel-Based Analogues. J Catal 269:80–92

57. Koeppel RA, Wehrli JT, Wainwright MS, Trimma DL, Cant NW (1994) Selective Hydrogenation of C-4-alkynes over a Copper on Silica Catalyst. Appl Catal 120:163–177
58. Che C, Wang B, Shan C, Chen H, Liu W, Tang Y (2017) An Effective Strategy to Prepare Pd-Ag/$MgCO_3$@alpha-$Al_2O_3$ Catalyst for Selective Hydrogenation of Acetylene. Catal Lett 147:483–490
59. Wehrli JT, Thomas DJ, Wainwright MS, Trimma DL, Cant NW (1991) Selective Hydrogenation of Propyne over Supported Copper Catalysts: Influence of Support. Appl Catal 70:253–262